Optics Letters

Controllable EIT-like mode splitting in a chiral microcavity

Guolin Zhao,[1] Jiefu Zhu,[1] Jiankun Hou,[2] Yao Chen,[2] Jintian Lin,[3] Ya Cheng,[3,4] Xianfeng Chen,[1] Yuanlin Zheng,[1] and Wenjie Wan[1,2,*]

[1]School of Physics and Astronomy, Shanghai Jiao Tong University, Shanghai 200240, China
[2]University of Michigan-Shanghai Jiao Tong University Joint Institute, Shanghai Jiao Tong University, Shanghai 200240, China
[3]CAS Center for Excellence in Ultra-Intense Laser Science, Chinese Academy of Science, Shanghai 201800, China
[4]School of Physics and Electronic Science, East China Normal University, Shanghai 200241, China
*Corresponding author: wenjie.wan@sjtu.edu.cn

Received 5 December 2022; revised 28 December 2022; accepted 28 December 2022; posted 3 January 2023; published 26 January 2023

Two coupled resonance modes can lead to exotic transmission spectra due to internal interference processes. Examples include electromagnetically induced transparency (EIT) in atoms and mode splitting in optics. The ability to control individual modes plays a crucial role in controlling such transmission spectra for practical applications. Here we experimentally demonstrate a controllable EIT-like mode splitting in a single microcavity using a double-port excitation. The mode splitting caused by internal coupling between two counter-propagating resonances can be effectively controlled by varying the power of the two inputs, as well as their relative phase. Moreover, the presence of asymmetric scattering in the microcavity leads to chiral behaviors in the mode splitting in the two propagating directions, manifesting itself in terms of a Fano-like resonance mode. These results may offer a compact platform for a tunable device in all-optical information processing.

https://doi.org/10.1364/OL.482912

Electromagnetically induced transparency (EIT), first discovered in atomic physics, is a consequence of destructive interference between two quantum transitions in a multilevel atom [1]. It allows a narrow transparent window inside an opaque absorption dip, altering the transmission spectrum. Meanwhile, the corresponding phase spectrum has also been modified accordingly. These features enable many applications such as slowing light [2,3], light storage [4,5], and all-optical switching [6]. However, due to the rigid experimental conditions—such as vacuum and cryogenic conditions—to realize EITs in the atoms, it is difficult to implement EITs for practical applications. Alternatively, EIT-like spectra have also been realized in a high-Q whispering gallery mode resonator (WGMR) [7] platform, where EIT-like spectra can be obtained from the coherent interference between two individual whispering gallery mode (WGM) resonances from two coupled resonators [8–12]. But it is a demanding task that requires either fine fabrication or thermal control to ensure the two resonances coincide with each other. On the other hand, EIT-like spectra have also been demonstrated in a single WGMR through two nonlinear coupled resonances in the frequency domain, e.g., via four-wave mixing [13] and stimulated Brillouin scattering [14,15]. However, strong nonlinearity and strict nonlinear phase-matching conditions are still required. So far, it remains a challenge to realize EIT in a single microcavity, preferably in a linear fashion.

It is well known that two counter-propagating modes in a WGMR can couple with each other, leading to a double resonance spectrum known as mode splitting [16,17]. This coupling mechanism can serve as an ideal platform for the realization of EIT-like spectra in a single microcavity. In this Letter, we experimentally demonstrate controllable EIT-like mode splitting in a single LiNbO3 microdisk cavity in the linear regime. Such mode splitting can be effectively controlled under a double-port excitation scheme, where the two inputs from opposite directions can linearly interfere and couple to each other inside the microcavity due to internal scattering. As a result, the EIT transmission spectra can be actively tunable by varying the power of the two inputs, as well as their relative phase. Moreover, the presence of an asymmetric scattering process in the current microcavity leads to chiral behaviors in the mode splitting in the two propagating directions, manifesting itself in terms of a Fano-like resonance mode. These results enable a coherent and tunable method to control the transmission through our compact photonic devices, paving the way for practical applications in all-optical information processing and sensitive optical sensors.

The mode splitting can be realized in a single microcavity. To encourage coherent control of two counter-propagating modes, two input lasers have to be launched from opposite directions. Figure 1 shows the experimental schematics: the continuous-wave signals from a tunable laser source (TLS) are equally divided into clockwise (CW) and counterclockwise (CCW) directions by a fiber coupler. Two variable optical attenuators (VOAs) and polarization controllers (PCs) control the power (0~Max) and polarization of the two branches, respectively. Two identical fiber couplers are inserted into the two branches for power monitoring. The CW and/or CCW signals are guided into a tapered fiber and evanescently tunnel into the neighboring microdisk resonator through this tapered fiber. The microdisk resonator is fabricated on a commercial lithium niobate-on-insulator (LNOI) wafer with a 300-nm thick x-cut lithium niobate layer and a diameter of 80 μm [details of fabrication are discussed elsewhere in Ref. 18]. The measured Q-factor

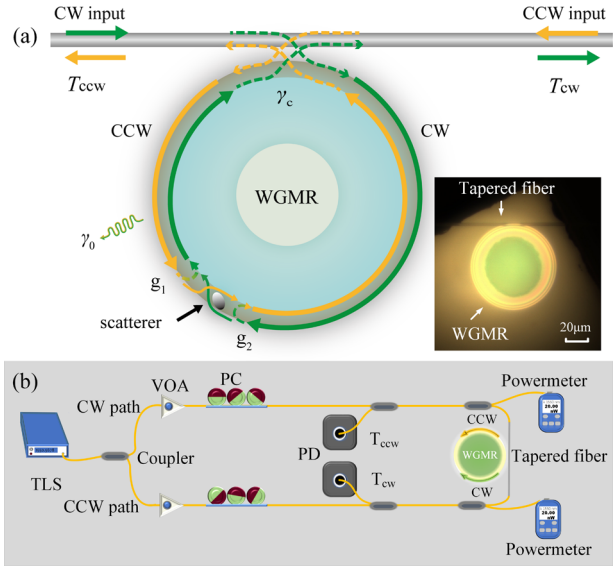

Fig. 1. Experimental setup of EIT-like mode splitting in a single microcavity. (a) Schematic illustration of bidirectional coupling-induced controllable EIT-like mode splitting model; inset is a micrograph of x-cut $LiNbO_3$ WGMR. (b) Schematic representation of the optical path: TLS, tunable laser source; VOA, variable optical attenuator; PC, polarization controller; PD, photodetector.

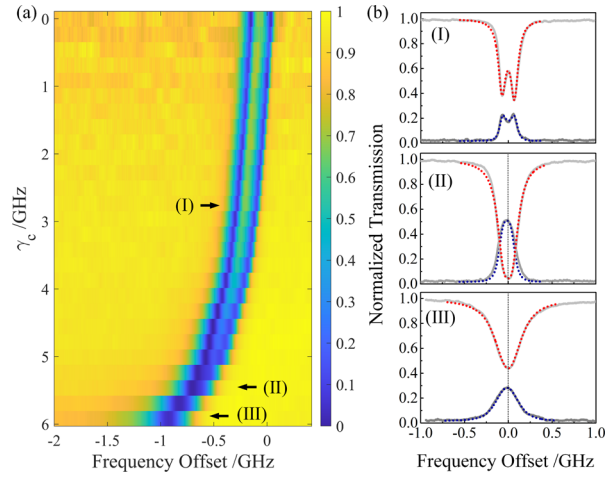

Fig. 2. Mode splitting in a single-port transmission. (a) Splitting transmission depends on the external coupling loss rate γ_c; all data normalized to [0, 1] to intuitively display the dynamic evolution of the splitting spectrum with respect to γ_c. (b) Branch CW transmission (upper) and reflection (lower) spectra of three coupling states corresponding to under-, critical-, and over-coupling; dotted lines are theoretical data; (g_1, g_2) are (0.476 GHz, 0.435 GHz), (0.39 GHz, 0.35 GHz), and (0.32 GHz, 0.30 GHz), respectively.

is around 10^6 for the input 1550-nm laser. The resonator is placed on the precision 3D piezoelectric stage with 20-nm resolution to adjust the coupling gap between the resonator and tapered fiber.

Figure 2 shows the single-port transmission spectra through our microcavity. Evidently, the EIT-like mode splitting is clearly visible in Fig. 2(b). The surface imperfections and scatterers on the edge of the microcavity naturally give rise to the internal coupling between the counter-propagating CW and CCW modes, causing a doublet in the form of two resonant dips to appear in the transmission spectrum [Fig. 2(b)(I)]. As shown in Fig. 2(a), the observed doublet dips gradually approach each other when reducing the coupling gap, and finally emerge into one single resonance dip in the critical-coupling regime. This occurs because the extra perturbation in the critical- and over-coupling regime brings in additional coupling loss, which finally makes the resonance linewidth broader than the mode splitting. The feature allows us to control the splitting transmission spectrum of the resonator by adjusting the coupling gap. Note that as more laser power is coupled into the cavity, this results in the redshift of the resonant frequency. Figure 2(b) shows transmission and reflection spectra of the three coupling states labeled in (a), corresponding to under-, critical-, and over-coupling of the perfect WGM cavity.

Theoretically, when considering double-port excitation, the varying field amplitude of CW and CCW modes can be described by the temporal coupled-mode theory [19]:

$$\frac{da_{cw}}{dt} = (i\Delta\omega - ig_1 - \gamma)a_{cw} + ig_2 a_{ccw} + \sigma a_{cw}^{in} \quad (1)$$

$$\frac{da_{ccw}}{dt} = (i\Delta\omega - ig_2 - \gamma)a_{ccw} + ig_1 a_{cw} + \sigma a_{ccw}^{in}, \quad (2)$$

where a and a^{in} are the amplitude of CW and CCW modes of the resonator and the input field, respectively.$\Delta\omega$ is detuning with respect to resonance angular frequency.$\gamma = \gamma_0 + \gamma_c$, where γ_0 is intrinsic loss rate and γ_c is external coupling loss rate of the resonator.$\sigma = \sqrt{2\gamma_c/\tau}$ is the coupling rate of the input wave to modes of the resonator, where τ denotes the time for one round trip. g is the backscattering coupling coefficient. Under the static assumption, the coupling of the resonator modes to the tapered fiber gives rise to two transmitted fields:

$$T_{cw} = [(a_{cw}^{in} - \sigma\tau a_{cw})/a_{cw}^{in}]^2, \; T_{ccw} = [(a_{ccw}^{in} - \sigma\tau a_{ccw})/a_{cw}^{in}]^2. \quad (3)$$

Obviously, Eqs. (1)–(3) indicate that such transmission spectra highly depend on the input signal ratio between the opposite input direction. Under double-port excitation, as shown in Fig. 1, two input beams can be launched simultaneously from both ports into the microcavity. In this manner, we can utilize the signal in one direction to control the transmission spectrum in the other. Initially, the single-port transmission spectrum is obtained as the Lorentz line shape with ~45-nW laser input along the CW direction in the critical-coupling regime [left panel of Fig. 3(a)]. Gradually increasing the power of the CCW branch to 16.6 nW, the coupling between CW and CCW modes lifts their degeneracy and appears as double dips in the transmission spectrum in Fig. 3(a). This EIT-like transmission clearly demonstrates the nature of the interference and fits well with the theoretical results from Eq. (3).

In this manner, we can artificially induce mode splitting by simultaneously inputting two beams of in-phase (we shall discuss it in the later section) laser with opposite directions in a non-splitting WGM resonator. By further increasing the input power of the CCW branch, the field intensity of the CCW mode in the cavity can be further enhanced. The resulting transmission spectra are shown in Fig. 3(a) and splitting spike intensity versus the input power ratio, i.e., $\eta = P_{ccw}/P_{cw}$ shown in Fig. 3(b). This rising spike in the EIT-like spectra indicates the clear interference between the CW and CCW modes, enabling active switching dynamics of EIT through simple double input control.

More interestingly, we experimentally observe the strong asymmetric backscattering of WGM which depends on the

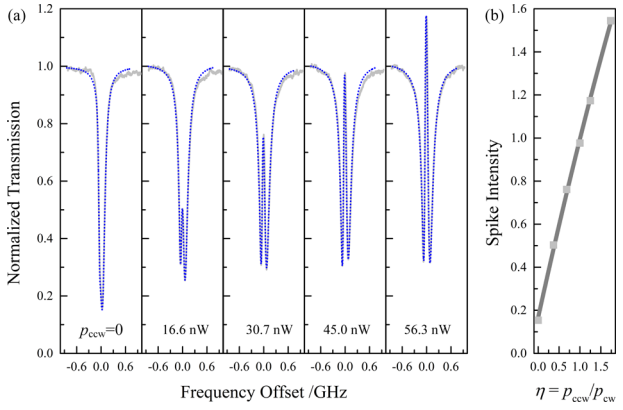

Fig. 3. Controllable EIT-like transmission when varying the CW/CCW input power ratio. (a) CW transmission spectra at different powers of CCW input; the blue dotted lines are theoretically fitted by Eq. (3), the CCW input power increases from left to right. (b) Dependence of the spike intensity of CW direction on power ratio η; the solid line is fitted by Eq. (3).

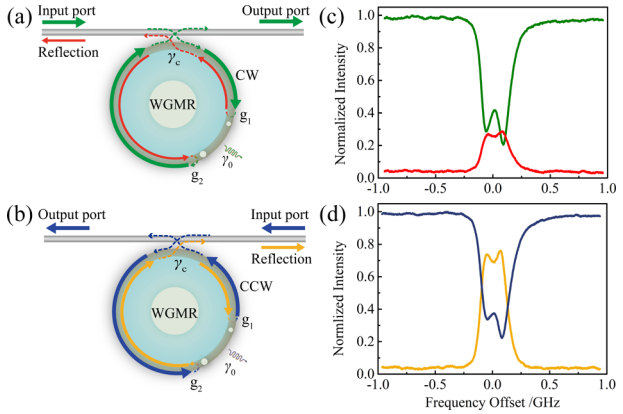

Fig. 4. (a) and (b) Schematic representations of two configurations of a single-input port structure which consists of one coupling fiber and one micro-resonator. (c) and (d) Transmission and reflection spectra belonging to the two configurations. A special mode with a wavelength of 1540.38 nm is chosen for demonstrating chiral backscattering; a scanning laser signal with a power of 53.62 nW is fed into two ports of the tapered fiber and the consequent reflection spectra, with a difference of 2.65 times (normalized), are obtained in (c) and (d).

incident direction of the laser signal, namely chiral reflection [20,21]. Figure 4 schematically shows two scenarios of single-port transmission and reflection spectra through the same microcavity from two opposite directions, while the two transmission spectra [Figs. 4(c) and (d)] remain similar to each other due to the reciprocity. However, their reflection spectra differ by more than two times, reflecting the chiral behavior in the current microcavity, i.e., $g_1 \neq g_2$ in Eq. (1). Fundamentally, such asymmetric backscattering in the CW and CCW direction is caused by the broken azimuthal symmetry, e.g., different sizes of the two scatters on the microcavity's rim [22], as shown in Figs. 4(a) and 4(c). These scatters may originate during the fabrication process or afterward, and their relative positions on the microcavity play a crucial role in determining the asymmetric reflections [20,22]. As a result, such intrinsic chiral reflection can intuitively lead

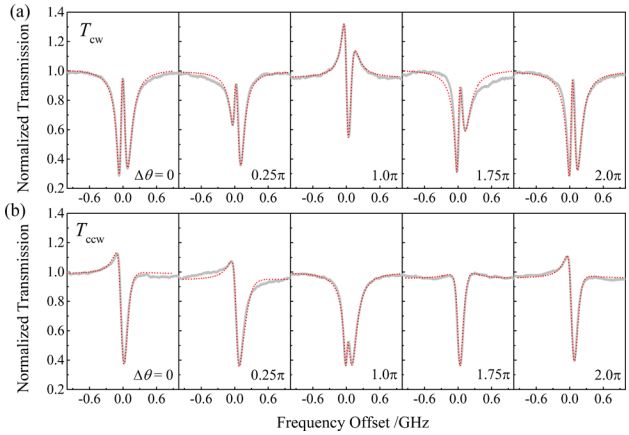

Fig. 5. Coherent control of EIT-like mode splitting when both the power of CW and CCW are fixed at 45 nW. Upper panels (a) are CW transmission spectra, and the lower panels (b) are CCW transmission spectra. Dotted lines are calculated by Eq. (3). The phase differences $\Delta\theta$ are labeled in the subgraphs.

to the asymmetric mode splitting in two directions when the double-port excitation is implemented.

Under the double-port excitation scheme, the relative phase between CW and CCW input signals plays a critical role in artificially induced mode splitting. We define $a_{ccw}^{in} = \sqrt{\eta} a_{cw}^{in} e^{-i\Delta\theta}$, where $\Delta\theta$ is the phase difference between CW and CCW laser light. To demonstrate the coherent control of two-port EIT-like mode splitting, we simultaneously launch two beams with equal power from both ports into the microcavity and heat the CCW arm's fiber with a thermoelectric cooler (TEC) to change its refractive index and thus control the relative phase [23].

Figure 5 illustrates the synchronous evolution of CW (upper) and CCW (lower) transmission spectra, depending on their phase difference within $0 \sim 2\pi$. At $\Delta\theta = 0$, the CW transmission remains an EIT-like spectrum, while its counterpart in the CCW direction is slightly distorted into a Fano-like resonance [13]. This reflects the fact the asymmetric coupling induces an extra phase delay. When varying this phase difference between the CW/CCW inputs, we do observe the spectrum change in both CW and CCW directions in Fig. 5, some of them being highly asymmetric in the spectrum, ranging from a typical EIT-like, Lorentz line shape with linewidth narrowing 75 MHz of T_{ccw} at $\Delta\theta = 1.75\pi$, and even a double Fano resonance of T_{cw} at $\Delta\theta = \pi$. All of these features can be caught with our theoretical model in Eq. (3) by introducing the phase difference between the two inputs. This opens the door for coherent controlling of EIT in all-optical information processing.

In conclusion, we experimentally demonstrate a controllable EIT-like mode splitting in a single microcavity using a double-port excitation. The mode splitting is sensitive to both the power of the two inputs and their relative phase. In this manner, the signal from one port can efficiently control the transmission of the signal from the other in a linear fashion, effectively constructing an all-optical-modulation scheme, which is crucial for all-optical computing and all-optical information applications. On the other hand, such mode splitting is also phase-sensitive, dramatically altering their transmission spectra. In the future, we may implement such a device as a sensitive phase detector to sense two inputs' small relative phase jumps, which may be caused externally through temperature, stress, or other means. In summary,

our results may pave the way for on-chip all-optical control, sensitive sensing, and precision measurement in a low-cost and compact form.

Funding. National Natural Science Foundation of China (11304201, 12274295, 92050113).

Disclosures. The authors declare no conflicts of interest.

Data availability. Data underlying the results presented in this paper are not publicly available at this time but may be obtained from the authors upon reasonable request.

REFERENCES

1. K. J. Boller, A. Imamoglu, and S. E. Harris, Phys. Rev. Lett. **66**, 2593 (1991).
2. L. V. Hau, S. E. Harris, Z. Dutton, and C. H. Behroozi, Nature **397**, 594 (1999).
3. M. F. Yanik, W. Suh, Z. Wang, and S. H. Fan, Phys. Rev. Lett. **93**, 233903 (2004).
4. D. F. Phillips, A. Fleischhauer, A. Mair, R. L. Walsworth, and M. D. Lukin, Phys. Rev. Lett. **86**, 783 (2001).
5. A. V. Turukhin, V. S. Sudarshanam, M. S. Shahriar, J. A. Musser, B. S. Ham, and P. R. Hemmer, Phys. Rev. Lett. **88**, 023602 (2001).
6. A. W. Brown and M. Xiao, Opt. Lett. **30**, 699 (2005).
7. D. K. Armani, T. J. Kippenberg, S. M. Spillane, and K. J. Vahala, Nature **421**, 925 (2003).
8. Q. F. Xu, S. S. Hu, M. L. Povinelli, J. Shakya, S. H. Fan, and M. Lipson, Phys. Rev. Lett. **96**, 123901 (2006).
9. C. H. Dong, C. L. Zou, Y. F. Xiao, J. M. Cui, Z. F. Han, and G. C. Guo, J. Phys. B: At., Mol. Opt. Phys. **42**, 215401 (2009).
10. Y. F. Xiao, L. N. He, J. G. Zhu, and L. Yang, Appl. Phys. Lett. **94**, 231115 (2009).
11. B. B. Li, Y. F. Xiao, C. L. Zou, Y. C. Liu, X. F. Jiang, Y.-L. Chen, Y. Li, and Q. Gong, Appl. Phys. Lett. **98**, 021116 (2011).
12. S. X. Yuan, L. Chen, Z. W. Wang, R. L. Wang, X. J. Wu, and X. L. Zhang, Appl. Phys. Lett. **115**, 201102 (2019).
13. Y. L. Zheng, J. F. Yang, Z. H. Shen, J. J. Cao, X. F. Chen, X. G. Liang, and W. J. Wan, Light: Sci. Appl. **5**, e16072 (2016).
14. F. X. Zhang, Y. M. Feng, X. F. Chen, L. Ge, and W. J. Wan, Phys. Rev. Lett. **124**, 053901 (2020).
15. T. Qin, J. Yang, F. Zhang, Y. Chen, D. Shen, W. Liu, L. Chen, X. Jiang, X. Chen, and W. Wan, Commun. Phys. **3**, 118 (2020).
16. T. J. Kippenberg, S. M. Spillane, and K. J. Vahala, Opt. Lett. **27**, 1669 (2002).
17. D. S. Weiss, V. Sandoghdar, J. Hare, V. L. Seguin, J. M. Raimond, and S. Haroche, Opt. Lett. **20**, 1835 (1995).
18. X. N. Ye, S. J. Liu, Y. P. Chen, Y. L. Zheng, and X. F. Chen, Opt. Lett. **45**, 523 (2020).
19. L. N. He, S. K. Ozdemir, Y. F. Xiao, and L. Yang, IEEE J. Quantum Electron. **46**, 1626 (2010).
20. J. Wiersig, Phys. Rev. A **89**, 012119 (2014).
21. B. Peng, S. K. Özdemir, M. Liertzer, W. Chen, J. Kramer, H. Yilmaz, J. Wiersig, S. Rotter, and L. Yang, Proc. Natl. Acad. Sci. **113**, 6845 (2016).
22. J. Hou, J. Lin, J. Zhu, G. Zhao, Y. Chen, F. Zhang, Y. Zheng, X. Chen, Y. Cheng, L. Ge, and W. Wan, PhotoniX **3**, 22 (2022).
23. L. Jiang, J. Yang, S. Wang, B. Li, and M. Wang, Opt. Lett. **36**, 3753 (2011).